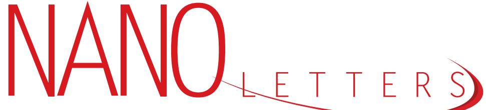

Letter

pubs.acs.org/NanoLett

Intercalation Doped Multilayer-Graphene-Nanoribbons for Next-Generation Interconnects

Junkai Jiang,[†] Jiahao Kang,[†] Wei Cao,[†] Xuejun Xie,[†] Haojun Zhang,[†] Jae Hwan Chu,[†] Wei Liu,[†] and Kaustav Banerjee*,[†]

[†]Department of Electrical and Computer Engineering, University of California, Santa Barbara, California 93106, United States

Supporting Information

ABSTRACT: Copper-based interconnects employed in a wide range of integrated circuit (IC) products are fast approaching a dead-end due to their increasing resistivity and diminishing current carrying capacity with scaling, which severely degrades both performance and reliability. Here we demonstrate chemical vapor deposition-synthesized and intercalation-doped multilayer-graphene-nanoribbons (ML-GNRs) with better performance (more than 20% improvement in estimated delay per unit length), 25%/72% energy efficiency improvement at local/global level, and superior reliability w.r.t. Cu for the first time, for dimensions (down to 20 nm width and thickness of 12 nm) suitable for IC interconnects. This is achieved through a combination of GNR interconnect design optimization, high-quality ML-GNR synthesis with precisely controlled number of layers, and effective $FeCl_3$ intercalation doping. We also demonstrate that our intercalation doping is stable at room temperature and that the doped ML-GNRs exhibit a unique width-dependent doping effect due to increasingly efficient $FeCl_3$ diffusion in scaled ML-GNRs, thereby indicating that our doped ML-GNRs will outperform Cu even for sub-20 nm widths. Finally, reliability assessment conducted under accelerated stress conditions (temperature and current density) established that highly scaled intercalated ML-GNRs can carry over 2×10^8 A/cm^2 of current densities, whereas Cu interconnects suffer from immediate breakdown under the same stress conditions and thereby addresses the key criterion of current carrying capacity necessary for an alternative interconnect material. Our comprehensive demonstration of highly reliable intercalation-doped ML-GNRs paves the way for graphene as the next-generation interconnect material for a variety of semiconductor technologies and applications.

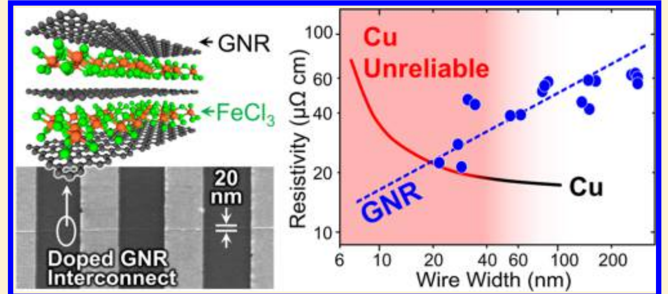

KEYWORDS: *Graphene, graphene-nanoribbon, intercalation doping, interconnect, Raman spectroscopy, contact resistance, breakdown, resistivity*

Metal interconnects based on Cu suffer from significant size-effects, including surface and grain boundary scatterings, when their width is scaled below 40 nm, leading to a strongly nonlinear increase in their resistivity (Supporting Information S1), which increases self-heating, degrades electromigration (EM) reliability (Figure S1e in the Supporting Information), and thereby limits their current carrying capacity[1−3] (Figure 1a). The relatively thick and highly resistive barrier layer that prevents Cu diffusion into dielectric layers also contributes to the rapid increase of the resistivity.[2] Recently, graphene was proposed to be used as diffusion barrier for Cu.[4,5] Although the elimination of conventional TaN/TiN barrier layer by using a single-layer-graphene (SLG) barrier reduces the effective resistivity of Cu, the fundamental reliability problem arising from EM and self-heating remains unsolved (Figure 1a). Use of other metals exhibiting lesser degree of size-effects suffers from the same limitation, while more disruptive solutions, such as on-chip optical interconnects, are impractical for the scaled interconnect levels.[6]

Graphene is a single sheet of carbon atoms, arranged in a hexagonal lattice,[7] and held together by strong in-plane sp^2 bonds. It has attracted tremendous research since its first demonstration.[8] Owing to its outstanding electrical,[9] optical, and thermo-mechanical[10] properties, various graphene devices have been demonstrated in multiple fields, including electriconic devices,[11,12] optical modulators,[13] etc. By stacking multilayers of graphene with van der Waals bonding and patterning it into few tens of nanometers wide ribbons, multilayer (ML)-GNR offers a promising solution to the above interconnect scaling issues. This is primarily because of the experimentally confirmed high current carrying capacity (>100 MA/cm^2 in few-layer graphene[14,15]). However, in a realistic nanoscale ML-GNR interconnect, its conductivity is limited due to additional carrier scatterings, including intersheet electron hopping, reduced carrier mean free path from edge scatterings, and bandgap opening for sub-20 nm widths[16] (Figure S1b in Supporting Information). To overcome these challenges, intercalation-doped ML-GNR interconnect was first

Received: October 28, 2016
Revised: December 20, 2016
Published: December 22, 2016

© 2016 American Chemical Society

DOI: 10.1021/acs.nanolett.6b04516
Nano Lett. 2017, 17, 1482−1488

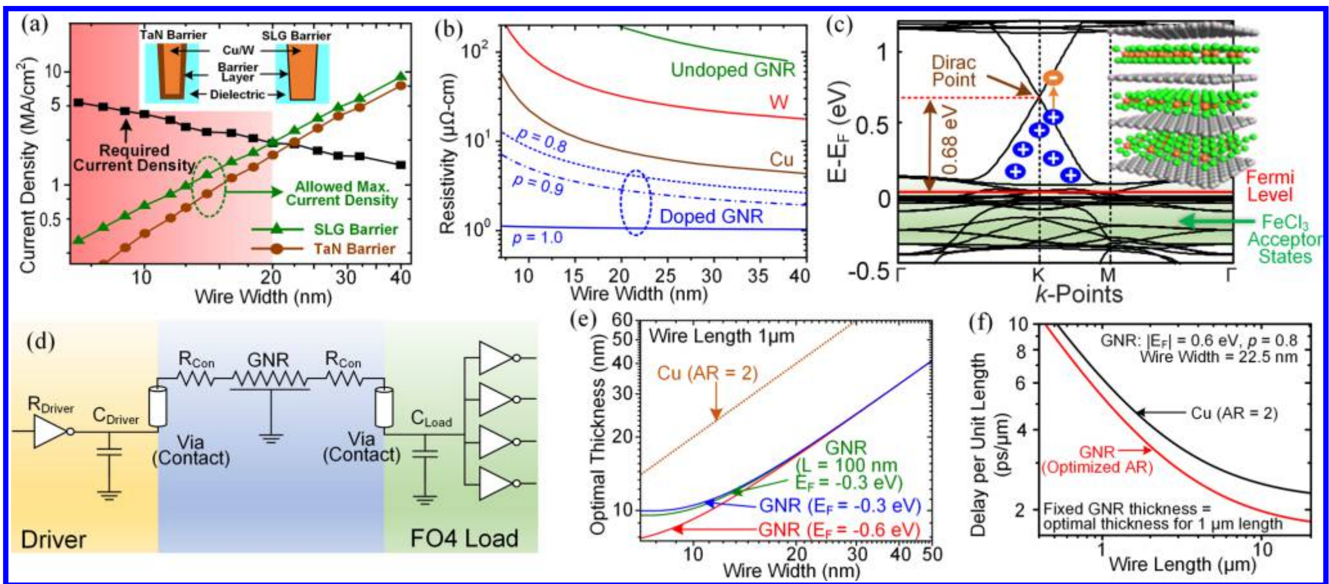

Figure 1. (a) Circuit-performance required current density for integrated circuit interconnects and the maximum allowed current density for Cu interconnects with TaN and SLG barrier (from EM reliability and self-heating). The red region indicates that the required current density exceeds the maximum allowed current density as interconnect scales down. The inset figures show the cross-sectional schematic of Cu interconnect with TaN and SLG barrier layer. (b) Theoretical estimation showing that doped GNR's resistivity can beat that of Cu and W (both with 1.9 nm barrier layer) with doping level $E_F = -0.6$ eV and edge specularity coefficient $p \geq 0.8$. (c) Band structure of stage-1 $FeCl_3$ intercalation doped ML-graphene (inset figure). The maximum doping level (at stage-1 intercalation) is $E_F = -0.68$ eV. The band structure for ML-GNRs remain similar to (c) down to GNR width of 20 nm.[18] (d) Schematic of an inverter driving a fan-out-of-four (FO4) load through a GNR interconnect. R_{driver} is the driver effective resistance, C_{driver} and C_{load} represent the effective driver and load capacitances, respectively, and R_{con} is the contact resistance between GNR and metal. Values of various parameters used in delay optimization are listed in Fig. S3a in the Supporting Information. (e) The optimized thickness for a typical 1 μm long (about 20−50 times the transistor size) GNR, by minimizing the wire delay in (d) for two different doping levels ($E_F = -0.3$ and −0.6 eV). The optimized thickness for GNR length of 100 nm (green line) is similar to the 1 μm result (Supporting Information S3). The aspect ratio (thickness/width) AR = 2 line highlights the importance of the GNR's thickness optimization. Note that Cu interconnect optimized for delay (AR < 2) does not exhibit sufficient current carrying capacity to satisfy circuit performance requirements and, therefore, is not plotted. (f) From simulations, delay per unit length is reduced by the optimized GNR AR, compared with Cu interconnect with AR = 2 employed in current IC technology.

proposed by Xu et al.[17] and theoretically proved to beat the resistivity and performance of Cu[18] by appropriate intercalation doping level (Figure 1b) (also see Figure S1c,d in Supporting Information). Since then, few experimental attempts have been reported. However, they either used few-layer graphene that is not suitable for interconnect applications, did not involve doping that is critical for achieving necessary conductivity, or was not optimized for circuit performance, and no reliability and stability data were provided.[19−21] To date, there is no experimental work on doped GNRs that demonstrate both electrical conductivity enhancement and reliability improvement, which is necessary to establish the utility of GNRs as next-generation interconnect material. In this work, more than 100 ML-GNRs (Figure 2a−h) are fabricated based on a practical interconnect design, guided by circuit level simulations and optimization (Figure 1d−f), and the fabricated doped GNR interconnects are shown to exhibit comparable resistivity and estimated better performance (lower delay per unit length) w.r.t. Cu with identical dimensions. For the first time, a width-dependent resistivity for undoped ML-GNR, consistent with theory,[18] and a unique width-dependent doping level for doped ML-GNR were observed. The time-to-fail (TTF) under accelerated stress conditions was measured, and superior reliability/current carrying capacity of GNR interconnects was identified.

Unique properties of ML-GNR, including extremely high current carrying capacity, make the conventional interconnect design approaches ineffective for maximizing the advantages of GNR interconnects. Hence, a circuit-level interconnect simulation and optimization specific to GNR is necessary. Based on the Landauer formalism, which accounts for edge scatterings and bandgap opening in narrow GNRs,[18] the conductivity of ML-GNR is calculated (Figure 1b). Additionally, the GNR quantum capacitance is found to be more than 1 order of magnitude larger than the electrostatic capacitance (Figure S2a,b in Supporting Information), and the impedance due to magnetic and kinetic inductance[22] is much smaller than the resistance for scaled local levels (Figure S2c in Supporting Information). Therefore, quantum capacitance and magnetic/kinetic inductance are neglected. Our circuit level simulation optimizes the GNR thickness by minimizing the wire delay of a unit-size inverter driving an FO4 load (Figure 1d). The optimized doped GNR interconnect offers better performance (up to more than 20% improvement in delay per unit length) than Cu (Figure 1f) and satisfies the current density required for circuit performance (Figure S3b in Supporting Information). Optimal thickness is found to be ∼10−15 nm for sub-20 nm width GNRs with moderate doping level ($|E_F| = 0.3$ eV, as observed in the experiments in Figure 3d) (Figure 1e), which is different from that of Cu interconnects with a typical aspect ratio (AR = thickness/width) of around 2, and this serves as a guideline for the subsequent experiments. The reduced optimal thickness in GNR arises due to their significantly reduced capacitance, which in turn reduces the delay. The reduced thickness of GNR is allowed by its superior current carrying

DOI: 10.1021/acs.nanolett.6b04516
Nano Lett. 2017, 17, 1482−1488

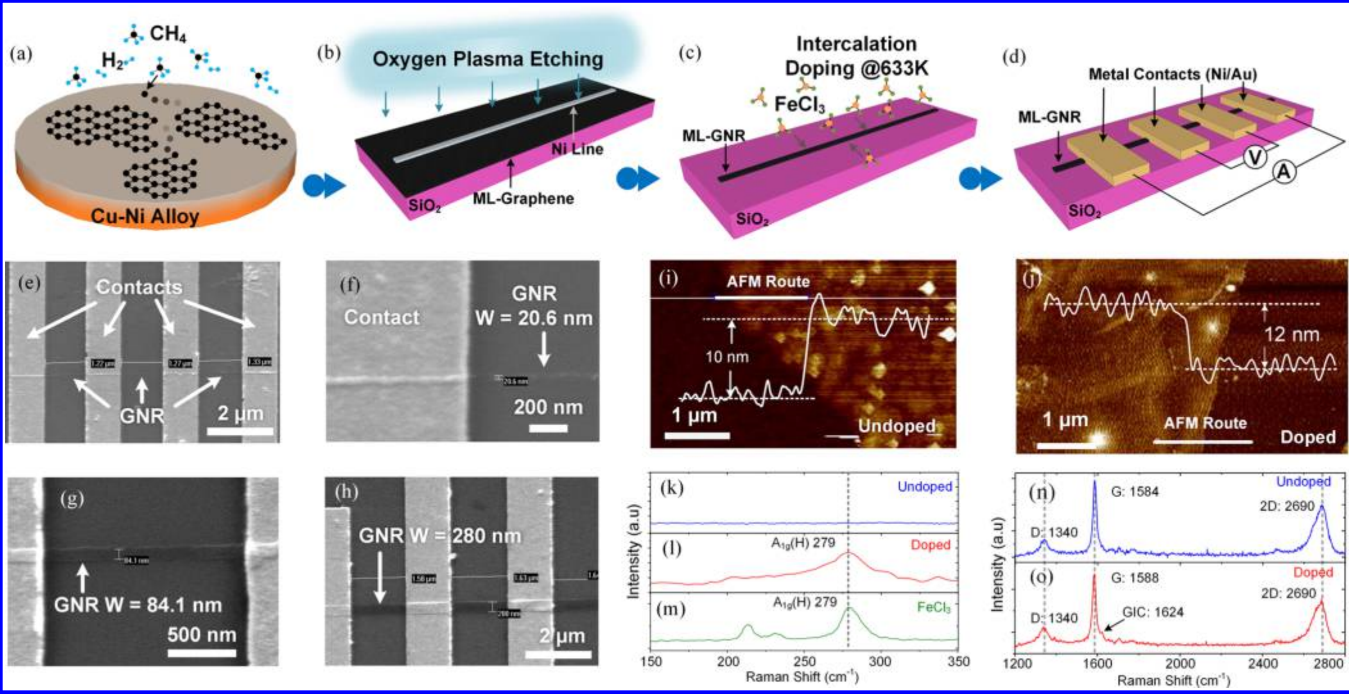

Figure 2. (a) Schematic of ML-graphene growth on Cu−Ni alloy catalyst by carbon surface segregation. (b) Transferred ML-graphene on SiO_2 and oxygen plasma etching with Ni line mask. (c) $FeCl_3$ intercalation doping in Ar atmosphere at 633 K and 1.0−1.4 atm. (d) 4-probe test structure. (e,f) SEM images of 4-probe test structure, with patterned GNR with 20.6 nm width. SEM image of GNR with (g) 84.1 nm and (h) 280 nm width. AFM image of (i) undoped ML-graphene and (j) 10-h $FeCl_3$ intercalation doped ML-graphene, indicating a 20% increase in thickness after intercalation doping. The Raman spectrum of (k,n) undoped ML-graphene, (l,o) $FeCl_3$ intercalation doped ML-graphene, and (m) $FeCl_3$. D, G, and 2D peaks are marked, indicating ML-graphene and the existence of defects normally observed in CVD ML-graphene. The $A_{1g}(H)$ Raman peak[34] is identified in both intercalation doped ML-graphene and $FeCl_3$, indicating the existence of $FeCl_3$ in doped ML-graphene. The existence of GIC peak[26] also confirms the intercalation. A 633 nm wavelength laser was used in all the Raman measurements.

capacity w.r.t Cu that satisfies the required current density after delay optimization (Supporting Information S3).

In order to synthesize 10−15 nm thick ML-graphene, Cu−Ni alloy catalyst was used to precisely control the number of graphene layers by adjusting the Cu−Ni ratio.[23] A 99.8% purity Cu foil was electropolished, and Ni was deposited on Cu foil surface. Ni−Cu alloy was formed by annealing for 2 h, followed by 45 min chemical vapor deposition (CVD) process (Figure 2a). Hydrogen gas flow was kept constant during the annealing and growth step to reduce Cu/Ni oxides and counterbalance the oxidizing impurities in the chamber for high quality ML-graphene growth.[24] The existence of ML-graphene, after transferring to SiO_2 substrate, is confirmed by Raman (Figure 2n) measurements. The ML-graphene thickness is 10 nm, identified by atomic force microscope (AFM) (Figure 2i), and is suitable for the optimized interconnect designs obtained from the design optimization, even after accounting for small thickness increase after intercalation doping (Figure 2j).

Starting from the ML-graphene, GNRs were defined by electron beam lithography (EBL). Since negative photoresist hydrogen silsesquioxane (HSQ) creates undeveloped residue that is difficult to remove,[14,20] a low concentration positive resist PMMA A2 was used to define GNR patterns. A ∼20 nm thick Ni layer was deposited on PMMA after EBL, followed by lift-off process to create Ni lines, which were used as masks in the oxygen plasma etching (Figure 2b). Finally, the Ni lines were removed by diluted HCl, leaving GNRs from 280 nm down to around 20 nm in width (Figure 2e−h). High vacuum ($<1 \times 10^{-6}$ mbar) and low deposition rate (<0.3 Å/s) during Ni deposition were found to be favorable in creating continuous Ni lines. Relatively low electron beam accelerating voltage (30 kV) creates undercut in E-beam resist by scattering and helps lift-off process. An overetching of graphene by oxygen plasma helps create narrow GNRs,[27] and oxygen plasma introduces oxygen terminations to the GNR edges (Supporting Information S4).

Density functional theory (DFT) simulations (see details in Supporting Information S5) show that $FeCl_3$ intercalation doping introduces high p-type doping ($|E_F|$ = 0.68 eV maximum doping level for stage-1 doping) in ML-graphene (Figure 1c) because of charge transfer between $FeCl_3$ acceptor states and graphene. Hence, $FeCl_3$ intercalation doping is conducted on GNR to enhance its electrical conductivity. The doping process is performed under 633 K and ∼1.4 atm pressure in Ar atmosphere for 10 h in a titanium high-pressure reactor[25] (Figure 2c). The GNR samples and $FeCl_3$ powder were placed in the high-pressure reactor, followed by sealing the reactor, purging-and-refilling with Ar gas, and heating up to 633 K. $FeCl_3$ evaporates and diffuses in between the GNR layers under high temperature and pressure and acts as acceptors that increases hole concentration. The Raman (Figure 2k−o), AFM (Figure 2i,j), and backgate electrical measurements (Figure S6a in Supporting Information S6) confirmed the existence of intercalation doping.[26] The 4-probe test structure (Figure 2d) with Ni/Au contacts were defined by EBL after the doping process. The surface roughness of SiO_2 substrate and the line edge roughness (LER) of GNRs are increased by $FeCl_3$ condensation on SiO_2 surface and GNR edges during the intercalation doping process. The measured standard deviation of LER, σ(LER) is ∼2.5 and ∼4 nm for undoped and doped

DOI: 10.1021/acs.nanolett.6b04516
Nano Lett. 2017, 17, 1482−1488

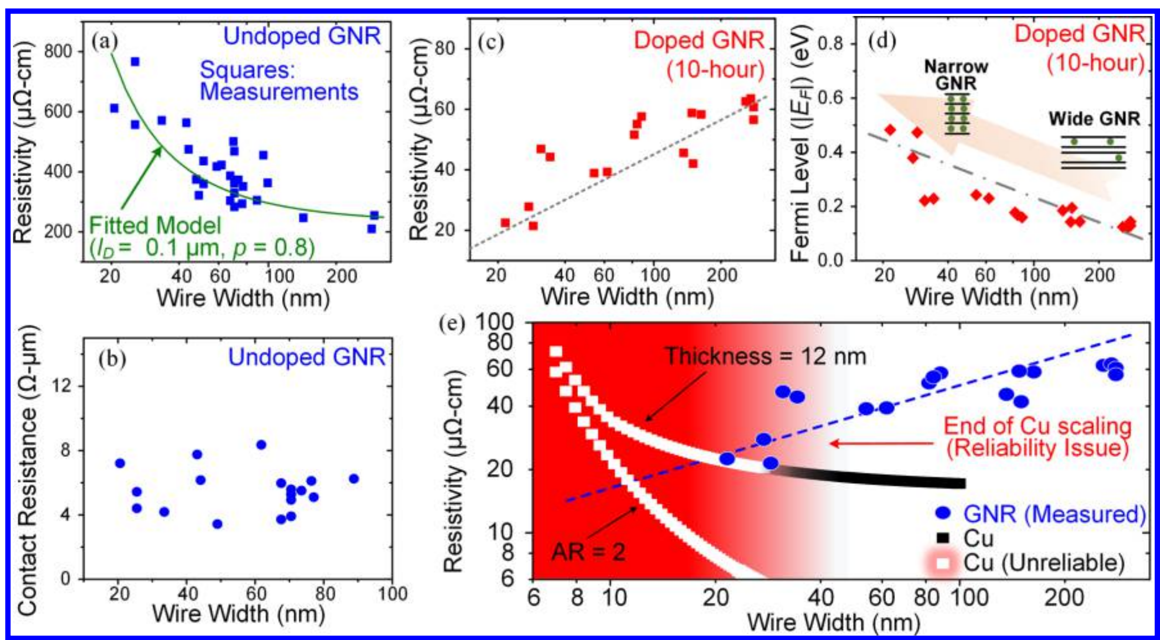

Figure 3. Measured resistivity of (a) undoped ML-GNR and (c) 10-h doped ML-GNR. (b) Measured undoped ML-GNR contact resistance. Similar contact resistance is observed for contact resistance in doped ML-GNR. (d) The extracted doping (Fermi) level for 10 h doped ML-GNR (Supporting Information S6). A higher doping level is observed for narrower GNRs. (e) Resistivity of Cu interconnect and doped GNR in this work, both of 12 nm thickness (as well as with AR = 2 for Cu). According to our coupled interconnect EM and self-heating simulation,[1] (Supporting Information S1) the Cu interconnects suffer from severe reliability issue (greatly diminished current carrying capacity w.r.t required current density), starting from ~40 nm width (highlighted region in red), when the thickness is the same (12 nm) for both GNR and Cu (similar reliability issue will be encountered for Cu of AR = 2 for sub-20 nm widths). Hence, Cu is unreliable for optimized sub-40 nm width interconnects, whereas doped ML-GNR offers similar resistivity for 20 nm width with a clear trend toward even lower resistivity values for sub-20 nm widths, with extraordinary current carrying capacity (shown in Figure 4).

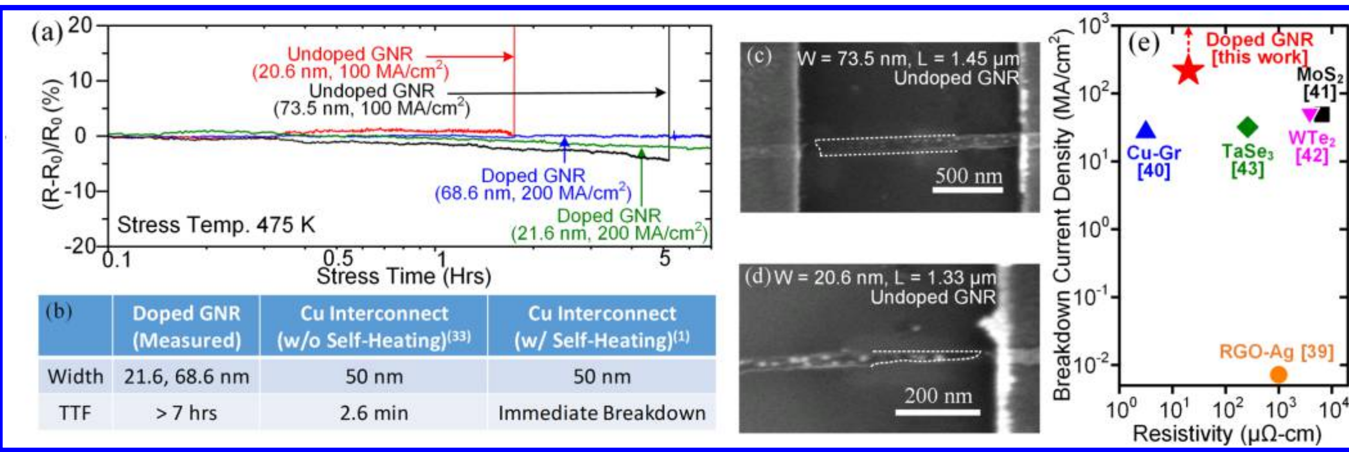

(b)	Doped GNR (Measured)	Cu Interconnect (w/o Self-Heating)(33)	Cu Interconnect (w/ Self-Heating)(1)
Width	21.6, 68.6 nm	50 nm	50 nm
TTF	> 7 hrs	2.6 min	Immediate Breakdown

Figure 4. (a) Breakdown measurements for undoped and doped GNR. The measured time-to-fail (TTF) for undoped GNR at 100 MA/cm^2 (DC stress) and 475 K is 1.8 hrs and 5.2 hrs for 20.6 and 73.5 nm width, respectively. No breakdown was observed for doped GNR (21.6 and 68.6 nm width) even under stress conditions of 200 MA/cm^2 and 475 K in 7 hrs. This establishes the outstanding reliability of $FeCl_3$ intercalation doped GNRs. (b) Summary of measured TTFs (using method outlined in Supporting Information S1) of doped GNR and estimated TTFs of Cu interconnect (with and without self-heating) under stress conditions in (a). (c,d) SEM images showing open circuit failures of undoped GNR from (a). The GNR is marked by dotted white lines. (e) Reported wire resistivity vs breakdown current density of possible candidate materials for scaled local interconnects. These materials include reduced-graphene-oxide (RGO)-Ag composite (wire width = 20 μm, measured in air[39]), ML-graphene-capped Cu (Cu-Gr) (wire width = 2 μm, measured in air[40]), semiconducting monolayer MoS_2 (wire width = 2 μm, encapsulated in dielectric[41]), semimetallic ML-WTe_2 (wire width = 2 μm, measured in vacuum[42]), metallic $TaSe_3$ (wire width ≈ 100 nm, encapsulated in hexagonal boron nitride[43]), and doped ML-GNR in this work. The resistivities of semiconducting materials are extracted for gate voltage V_G = 0 V. The breakdown current density of our doped ML-GNR is larger than 200 MA/cm^2, as indicated by the red dotted arrow.

GNR, respectively (by AFM measurements, Supporting Information S4). Nevertheless, the electrical conductivity increases for doped GNRs because the increase in LER scatterings is compensated by higher carrier concentration. Further increasing the intercalation doping time and pressure can potentially enhance GNR electrical conductivity. However, beyond the allowed maximum intercalation doping level (Figure 1c), additional surface/edge roughness scatterings and surface $FeCl_3$ impurity scatterings will degrade GNR electrical conductivity.[28]

DOI: 10.1021/acs.nanolett.6b04516
Nano Lett. 2017, 17, 1482−1488

In this study, measurements were performed in vacuum ($<5 \times 10^{-5}$ mbar). The resistivity of undoped GNR from 4-probe measurement at room temperature increases as GNR width decreases, showing the size-effects, and is fitted by the GNR resistance model in Figure 1b (Figure 3a). The carrier diffusion length (l_D) depicts the scatterings by defects and phonons and is fitted as 0.1 μm (Figure 3a). This l_D reflects the quality of our CVD ML-graphene (as compared with $l_D \approx 1$ μm for exfoliated suspended graphene[29]) and is width independent. The edge specularity coefficient (p) describes the degree of edge scattering and is fitted as 0.8 (Figure 3a). The total effective scattering length ($l_{scatter_eff}$), which also accounts for the edge scattering, is extracted to be 44.13 nm for GNR width of 20 nm. If the GNR width is scaled down to 2 nm, and by assuming the same carrier diffusion length (l_D) and edge specularity (p) in our calculations, the corresponding $l_{scatter_eff}$ is reduced to 15.27 nm, in agreement with the reported ~14 nm for ~2 nm wide bilayer GNR.[30] The contact resistance from 4-probe measurement for undoped (Figure 3b) and doped GNR is 4–8 $\Omega \cdot \mu$m. This low contact resistance is achieved by the selection of high work-function contact metal (Ni) and the ML-GNR that offers relatively large contact conduction by edge contacts.[31,32] $FeCl_3$ intercalation doping (10-h) increases the ML-GNR surface carrier concentration from 3.88×10^{13} cm^{-2} (undoped) to 1.75×10^{14} cm^{-2} (doped) (Supporting Information S6). 10-hrs doped GNRs (Figure 3c) show smaller resistivity than 5-h doped GNRs (Figure S6c,d in Supporting Information), indicating a higher doping level can be achieved by longer doping time. The extracted GNR doping levels (E_F) (Figure 3d) reveal that narrow GNRs are more strongly doped with $FeCl_3$, as $FeCl_3$ can diffuse in between GNR layers more efficiently in narrower GNRs. This width-dependent doping level promises a further decrease in resistivity for sub-20 nm GNRs. Our measured intercalation doped GNR resistivity is comparable w.r.t the Cu interconnect of the same AR (for 20 nm width), whereas sub-40 nm Cu interconnects can not sustain the circuit performance required current density for AR ≤ 2 (Figure 3e). By optimizing the intercalation doping process to achieve maximum (stage-1, Figure 1c) doping level and improving the quality of graphene ($I_D \sim 1$ μm), the doped GNR resistivity can be further reduced to < 6 $\mu\Omega$-cm at 20 nm width.[18] Note that the doped GNRs were kept in nitrogen atmosphere[34] and under vacuum environment at room temperature, and negligible change in the resistivity was observed after more than 2 weeks. This doping stability indicates that the above width-dependent doping level was not caused by unstable GNR surface/edge doping.[23]

Time-to-fail (TTF) of undoped and doped GNR interconnects were measured, under 475 K and 100 and 200 MA/cm^2 DC stress, respectively, which gives the worst case TTF (Figure 4a). GNR failure is defined as the moment when a rapid increase (>5×) of GNR resistance (Figure 4a) occurs. TTF is 1.8 h for a 20.6 nm wide undoped GNR and is 5.2 h for a 73.5 nm wide undoped GNR, showing a width dependence. No breakdown is observed for the doped GNR (21.6 and 68.6 nm widths) in the 7-h measurement, under 475 K and 200 MA/cm^2 DC stress because of the increased conductivity and smaller self-heating effect after $FeCl_3$ intercalation doping. The Cu interconnect TTF (Figure 4b) without considering self-heating effect is estimated from the reported data[33] for 50 nm wide Cu wires. Note that narrower Cu wires (~20 nm width, identical to the GNR in Figure 4a), suffer significantly more severely from EM because of Cu surface diffusion and thus have much smaller TTF. Furthermore, if the self-heating effect of Cu interconnect is considered, it will cause an immediate melting/breakdown under 200 MA/cm^2 stress[1] (Figure 4b). Therefore, the doped GNR interconnects offer unprecedented reliability improvement, whereas Cu interconnects suffer from immediate failure.

We note that no resistance increase over time was observed for both doped and undoped GNR during the stress test, indicating that electromigration, which is normally observed in Cu and creates voids that gradually grow and increase the wire resistance, did not contribute to GNR breakdown. Hence, the self-heating is the major factor that contributes to a thermally activated failure in case of undoped GNRs. The SEM images (Figure 4c,d) show that undoped GNR breakdown (in Figure 4a) spots are close to the contacts. This is likely caused by a combination of contact metal thermo-migration and/or fusion (metal extrusion observed in Figure 4c,d) and GNR thermal decomposition.[35] The existence of GNR thermal decomposition is confirmed by the reduced GNR width near the breakdown point after the stress test (Figure 4d). Note that the reported GNR breakdown mechanism in air is the oxidation of graphene at 873 K[35] and 563 K,[36] but in a practical interconnect design, where interconnects are encapsulated by dielectrics, the oxidation will not be a major factor. In case of the doped GNRs, absence of any degradation or failure under high current density and temperature stress, along with their lower resistivity, highlights their terrific potential as next-generation integrated circuit interconnects. Additionally, the current carrying capacity of GNRs can be further enhanced with high thermal conductivity dielectrics, like hexagonal boron nitride (h-BN)[37] and diamond,[38] which was demonstrated to support current density of >1 GA/cm^2, albeit in micrometer range graphene ribbons.

Compared with other candidate materials for scaled local interconnects, our doped-GNR shows advantage in terms of both resistivity and current carrying capacity (Figure 4e). Despite the advantage of spin-coating preparation, the reduced-graphene-oxde(RGO)/Ag composite is not preferable in terms of both electrical conductance and current carrying capacity.[39] MLG improves the current carrying capacity of Cu,[40] but as wire dimension scales, the MLG-capped Cu will suffer from edge/grain boundary scatterings, as discussed previously. Semiconducting van der Waals materials, like MoS_2, do not exhibit sufficient electrical conductivity for interconnect applications.[41] Other semimetallic or metallic van der Waals materials, like WTe_2[42]/$TaSe_3$,[43] offer moderate electrical conductivity, and their 2D/1D nature alleviates surface roughness scatterings at scaled dimensions. However, further enhancement of the electrical conductivity is prohibited by the limited carrier concentration, similar to undoped GNRs. Therefore, an applicable and stable doping method is desired for 2D/1D van der Waals materials' application in future interconnects.

In summary, $FeCl_3$ intercalation doped ML-GNR interconnects with width down to ~20 nm were demonstrated, with resistivity (21.45 $\mu\Omega$·cm) comparable w.r.t. Cu of the same thickness (Figure 3e), while providing extremely high current carrying capacity (no degradation after 7 h under 200 MA/cm^2 and 475 K stress condition) that Cu cannot compete with (Figure 4a,b). The achieved GNR resistivity at AR = 12 nm / 20 nm = 0.6 (Figure 3c) implies ~25% improvement in energy efficiency (switching energy per bit consumed by interconnects) compared with Cu interconnect of AR = 2 and of the

DOI: 10.1021/acs.nanolett.6b04516
Nano Lett. 2017, 17, 1482–1488

same width. Longer global interconnects (30 nm wide and 60 nm pitch) can allow ~72% energy savings by using doped ML-GNR interconnects (thickness of 12 nm) instead of Cu, under the same timing constraint (Supporting Information S3). A notable dependency of doping level on GNR width is identified, which indicates that for sub-20 nm widths, GNR's conductivity can be further enhanced to outperform Cu at those dimensions. Intercalation doped GNR's superior current carrying capacity demonstrated in this work enables optimized (smaller) aspect-ratio for lowering capacitance and improving circuit performance, and further scaling down of interconnects without encountering the reliability problem that plagues Cu and other metals. Besides the resistance to long-term migration/reliability issue, the doped-GNR also promises robustness against electrostatic discharge (ESD) induced failures that damages on-chip components, including interconnects.[44,45] Furthermore, by improving ML-graphene quality, optimizing the doping process, and using an encapsulation layer, the performance and energy efficiency can be further enhanced. Additionally, the superior in-plane thermal conductivity of ML-graphene w.r.t conventional interconnect materials can be judiciously exploited to alleviate on-chip hotspots, and further improve performance and reliability. This study firmly establishes the rationale and feasibility of employing doped ML-GNR interconnects in next-generation integrated circuits and paves the way for a carbon-based interconnect technology.

■ ASSOCIATED CONTENT

Supporting Information

The Supporting Information is available free of charge on the ACS Publications website at DOI: 10.1021/acs.nanolett.6b04516.

Simulations predicting GNR's resistivity w.r.t. Cu and current carrying capacity of Cu, GNR interconnect capacitance and inductance, GNR interconnect design optimization and power/energy consumption estimation, AFM study of GNR edge morphology, DFT analysis of undoped multilayer graphene, and GNR electrical measurements and analysis (PDF)

■ AUTHOR INFORMATION

Corresponding Author

*E-mail: kaustav@ece.ucsb.edu.

ORCID

Jae Hwan Chu: 0000-0002-1361-4445

Kaustav Banerjee: 0000-0001-5344-0921

Funding

This work was supported by Systems on Nanoscale Information fabriCs (SONIC), one of the six STARnet Centers, sponsored by MACRO and DARPA.

Notes

The authors declare no competing financial interest.

■ REFERENCES

(1) Banerjee, K.; Mehrotra, A. *IEEE Circuits and Devices Magazine* **2001**, *17* (5), 16–32.

(2) Im, S.; Srivastava, N.; Banerjee, K.; Goodson, K. E. *IEEE Trans. Electron Devices* **2005**, *52* (12), 2710–2719.

(3) Srivastava, N.; Banerjee, K. *JOM Journal of the Minerals, Metals and Materials Society* **2004**, *56* (10), 30–31.

(4) Mehta, R.; Chugh, S.; Chen, Z. *Nano Lett.* **2015**, *15* (3), 2024–2030.

(5) Li, L.; Chen, X.; Wang, C.-H.; Lee, S.; Cao, J.; Roy, S. S.; Arnold, M. S.; Wong, H.-S. *Symposium on VLSI Technology* **2015**, *8–4*, 1–2.

(6) Li, H.; Xu, C.; Banerjee, K. *IEEE Design and Test of Computers* **2010**, *27* (4), 20–31.

(7) Ajayan, P.; Kim, P.; Banerjee, K. *Phys. Today* **2016**, *69* (9), 38–44.

(8) Novoselov, K. S.; Geim, A. K.; Morozov, S. V.; Jiang, D.; Zhang, Y.; Dubonos, S. V.; Grigorieva, I. V.; Firsov, A. A. *Science* **2004**, *306* (5696), 666–669.

(9) Li, H.; Xu, C.; Srivastava, N.; Banerjee, K. *IEEE Trans. Electron Devices* **2009**, *56* (9), 1799–1821.

(10) Balandin, A. A. *Nat. Mater.* **2011**, *10* (8), 569–581.

(11) Lin, Y. M.; Dimitrakopoulos, C.; Jenkins, K. A.; Farmer, D. B.; Chiu, H. Y.; Grill, A.; Avouris, P. *Science* **2010**, *327* (5966), 662–662.

(12) Bae, S.; Kim, H.; Lee, Y.; Xu, X.; Park, J. S.; Zheng, Y.; Balakrishnan, J.; Lei, T.; Kim, H. R.; Song, Y. I.; Kim, Y. J. *Nat. Nanotechnol.* **2010**, *5* (8), 574–578.

(13) Liu, M.; Yin, X.; Ulin-Avila, E.; Geng, B.; Zentgraf, T.; Ju, L.; Wang, F.; Zhang, X. *Nature* **2011**, *474* (7349), 64–67.

(14) Murali, R.; Yang, Y.; Brenner, K.; Beck, T.; Meindl, J. D. *Appl. Phys. Lett.* **2009**, *94* (24), 243114.

(15) Li, H.; Russ, C. C.; Liu, W.; Johnsson, D.; Gossner, H.; Banerjee, K. *IEEE Trans. Electron Devices* **2014**, *61* (6), 1920–1928.

(16) Han, M. Y.; Ozyilmaz, B.; Zhang, Y.; Kim, P. *Phys. Rev. Lett.* **2007**, *98* (20), 206805.

(17) Xu, C.; Li, H.; Banerjee, K. *IEEE International Electron Devices Meeting (IEDM)* Dec 2008, 1–4. 10.1109/IEDM.2008.4796651.

(18) Xu, C.; Li, H.; Banerjee, K. *IEEE Trans. Electron Devices* **2009**, *56* (8), 1567–1578.

(19) Chen, X.; Lee, K.-J.; Akinwande, D.; Close, G. F.; Yasuda, S.; Paul, B.; Fujita, S.; Kong, J.; Wong, H.-S. *IEEE International Electron Devices Meeting (IEDM)* **2009**, 1–4.

(20) Katagiri, M.; Miyazaki, H.; Yamazaki, Y.; Zhang, L.; Matsumoto, T.; Wada, M.; Kajita, A.; Sakai, T. *IEEE International Interconnect Technology Conference (IITC)* **2013**, 1–3.

(21) Kondo, D.; Nakano, H.; Zhou, B.; I, A.; Hayashi, K.; Takahashi, M.; Sato, S.; Yokoyama, N. *IEEE International Interconnect Technology Conference (IITC)* **2014**, 1–3.

(22) Sarkar, D.; Xu, C.; Li, H.; Banerjee, K. *IEEE Trans. Electron Devices* **2011**, *58* (3), 843–852.

(23) Liu, W.; Kraemer, S.; Sarkar, D.; Li, H.; Ajayan, P. M.; Banerjee, K. *Chem. Mater.* **2013**, *26* (2), 907–915.

(24) Li, X.; Colombo, L.; Ruoff, R. S. *Adv. Mater.* **2016**, *28*, 6247–6252.

(25) Liu, W.; Kang, J.; Banerjee, K. *IEEE Electron Device Lett.* **2016**, *37* (9), 1246–1249.

(26) Enoki, T.; Suzuki, M.; Endo, M. *Graphite Intercalation Compounds and Applications*; Oxford University Press, 2003.

(27) Lian, C.; Tahy, K.; Fang, T.; Li, G.; Xing, H. G.; Jena, D. *Appl. Phys. Lett.* **2010**, *96* (10), 103109.

(28) Chen, J. H.; Jang, C.; Adam, S.; Fuhrer, M. S.; Williams, E. D.; Ishigami, M. *Nat. Phys.* **2008**, *4* (5), 377–381.

(29) Bolotin, K. I.; Sikes, K. J.; Hone, J.; Stormer, H. L.; Kim, P. *Phys. Rev. Lett.* **2008**, *101* (9), 096802.

(30) Wang, X.; Ouyang, Y.; Li, X.; Wang, H.; Guo, J.; Dai, H. *Phys. Rev. Lett.* **2008**, *100* (20), 206803.

(31) Khatami, Y.; Li, H.; Xu, C.; Banerjee, K. *IEEE Trans. Electron Devices* **2012**, *59* (9), 2444–2452.

(32) Khatami, Y.; Li, H.; Xu, C.; Banerjee, K. *IEEE Trans. Electron Devices* **2012**, *59* (9), 2453–2460.

(33) Khoo, K.; Tashiro, S.; Onuki, J. *Mater. Trans.* **2010**, *51* (7), 1183–1187.

(34) Zhao, W.; Tan, P. H.; Liu, J.; Ferrari, A. C. *J. Am. Chem. Soc.* **2011**, *133* (15), 5941–5946.

(35) Liao, A. D.; Wu, J. Z.; Wang, X.; Tahy, K.; Jena, D.; Dai, H.; Pop, E. *Phys. Rev. Lett.* **2011**, *106* (25), 256801.

DOI: 10.1021/acs.nanolett.6b04516
Nano Lett. 2017, 17, 1482–1488

(36) Chen, X.; Seo, D. H.; Seo, S.; Chung, H.; Wong, H. S. P. *IEEE Electron Device Lett.* **2012**, *33* (11), 1604−1606.
(37) Jain, N.; Bansal, T.; Durcan, C.; Yu, B. *IEEE Electron Device Lett.* **2012**, *33* (7), 925−927.
(38) Yu, J.; Liu, G.; Sumant, A. V.; Goyal, V.; Balandin, A. A. *Nano Lett.* **2012**, *12* (3), 1603−1608.
(39) Xu, Z.; Liu, Z.; Sun, H.; Gao, C. *Adv. Mater.* **2013**, *25* (23), 3249−3253.
(40) Kang, C. G.; Lim, S. K.; Lee, S.; Lee, S. K.; Cho, C.; Lee, Y. G.; Hwang, H. J.; Kim, Y.; Choi, H. J.; Choe, S. H.; Ham, M. H. *Nanotechnology* **2013**, *24* (11), 115707.
(41) Lembke, D.; Kis, A. *ACS Nano* **2012**, *6* (11), 10070−10075.
(42) Mleczko, M. J.; Xu, R. L.; Okabe, K.; Kuo, H. H.; Fisher, I. R.; Wong, H. S.; Nishi, Y.; Pop, E. *ACS Nano* **2016**, *10* (8), 7507−7514.
(43) Stolyarov, M. A.; Liu, G.; Bloodgood, M. A.; Aytan, E.; Jiang, C.; Samnakay, R.; Salguero, T. T.; Nika, D. L.; Rumyantsev, S. L.; Shur, M. S.; Bozhilov, K. N.; Balandin, A. A. *Nanoscale* **2016**, *8*, 15774−15782.
(44) Banerjee, K.; Amerasekera, A.; Hu, C. *34th Annual Proceedings, IEEE Reliability Physics Symposium* April 1996, 237−245. 10.1109/RELPHY.1996.492126.
(45) Banerjee, K.; Amerasekera, A.; Cheung, N.; Hu, C. *IEEE Electron Device Lett.* **1997**, *18* (9), 405−407.

DOI: 10.1021/acs.nanolett.6b04516
Nano Lett. 2017, 17, 1482−1488